16TH EUROPEAN CONFERENCE ON EARTHQUAKE ENGINEERING THESSALONIKI 18 - 21 JUNE 2018

PARALLEL COMPUTATION OF SEISMIC RESPONSE OF HIGH ARCH DAMS

Shengshan GUO[1], Deyu LI[2], Jin TU[3], Houqun CHEN[4]

ABSTRACT

The present paper deals with parallelization of nonlinear explicit dynamic finite element simulation on distributed memory computers with domain decomposition and explicit message passing for seismic response of arch dams. The parallel computation program is developed based on the combination of Fortran90 and MPI. The dynamic analysis model including explicit dynamic finite element method, viscoelastic artificial boundary, nonlinear effects of contact boundary and constitutive model is introduced. The parallelization strategy for nonlinear explicit dynamic finite element method is discussed. The efficiency of the proposed approach is demonstrated on the supercomputer of 'TH-1A'. The seismic response of two high arch dams is performed with the application of the program and two possible seismic failure modes of arch dams are revealed.

Keywords: high arch dam; seismic response; parallel computation; failure mode

1. INTRODUCTION

West China is rich in hydropower resource, which is also a strong earthquake area. With the hydropower development in this area where several 300-meter-level super high arch dams have been or will be under construction, seismic safety often becomes a controlling condition (Guo S et al. 2016). All the following factors should be involved for more realistic prediction of seismic performance of arch dams, such as nonlinear contact due to the opening of the contraction joints and the slipping of the sliding surface of dam abutment rock block, the nonlinear constitutive model due to the damage of dam and foundation, energy dispersion of the far-filed foundation, and dynamic interactions of dam-foundation-reservoir system. Such demands may lead to a very complex geometric model with millions or tens of millions of DOFs for a high arch dam. Moreover, the nonlinear behaviors including contact boundary nonlinearity and material nonlinearity have to be taken into account. In the time domain, the computation speed has become the bottleneck for the solution of such a large-scale nonlinear dynamic problem. For example, it takes 34 days to complete the seismic computation of Shapai arch dam with 1.2 million DOFs by serial computation, which is unacceptable for the engineering community.

Working together of multiple processors in parallel for a single application can greatly increase the computation speed of large-scale nonlinear dynamic finite element analysis. Belytschko et al. (1991)

[1]Doctor; Senior engineer, China institute of water resources and hydropower research; State Key Laboratory of Simulation and Regulation of Water Cycle in River Basin, Beijing, China, 305265331@qq.com
[2]Professor, China institute of water resources and hydropower research; State Key Laboratory of Simulation and Regulation of Water Cycle in River Basin, Beijing, China, lideyu@iwhr.com
[3]Professor, China institute of water resources and hydropower research; State Key Laboratory of Simulation and Regulation of Water Cycle in River Basin, Beijing, China, tujin@iwhr.com
[4]Professor, China institute of water resources and hydropower research; State Key Laboratory of Simulation and Regulation of Water Cycle in River Basin, Beijing, China, chenhq@iwhr.com

described the implementation of explicit finite element methods with contact-impact using a Single Instruction Multiple Data (SIMD) and data parallel approaches on Connection Machine computers. As the appearance of message passing libraries, such as Message Passing Interface (MPI), general purpose explicit dynamic finite element codes using Single Program Multiple Data (SPMD) approach such as ParaDyn (Hoover et al. 1995) and PRONTO3D (Plimpton et al. 1996) were emerging. Danielson et al. (1998) presented a nonlinear explicit dynamic finite element code for use on scalable computers using SPMD approach, which was written entirely in Fortran 90, but used MPI for all interprocessor communication. Parallelization of explicit dynamic finite element was discussed (Fahmy et al. 1994; Malone et al. 1994; Namburu et al.1995; Clinckemaillie et al. 1997) and demonstrated as an enabling technology for higher computing runs completed in shorter time with domain decomposition and explicit message passing (Krysl et al. 2001) .

In this paper, the dynamic analysis model including explicit dynamic finite element method, viscoelastic artificial boundary, contact model, and nonlinear constitutive model is introduced firstly. Second, the adopted parallelization strategy for nonlinear dynamic finite element method is discussed. Third, taking Shapai arch dam as an example, the performance of parallel computation program of seismic response of high arch dam (PSDAP) developed by authors is tested. Fourth, the seismic response of two high arch dams is performed with the application of the program and two possible seismic failure modes of arch dams are revealed.

2. ANALYSIS MODEL

2.1 Explicit Dynamic Finite Element Method

The dynamic equation after finite element discretization：

$$\mathbf{M}\ddot{\mathbf{U}} + \mathbf{C}\dot{\mathbf{U}} + \mathbf{K}\mathbf{U} = \mathbf{F} \tag{1}$$

Where, $\mathbf{M}$, $\mathbf{C}$ and $\mathbf{K}$ are the mass, damping and stiffness matrixes respectively， and $\mathbf{F}$, $\ddot{\mathbf{U}}$, $\dot{\mathbf{U}}$ and $\mathbf{U}$ are the load, acceleration, velocity and displacement vectors respectively.

For large-scale nonlinear dynamical calculations, the decoupled explicit integration algorithm is more efficient. Thus, this paper adopts the decoupled explicit numerical integration format which combines the centre differential and unilateral differential method.

$$\dot{\mathbf{U}}_{\mathrm{n}} = \frac{\mathbf{U}_{\mathrm{n}} - \mathbf{U}_{\mathrm{n-1}}}{dt},\ \ddot{\mathbf{U}}_{\mathrm{n}} = \frac{\mathbf{U}_{\mathrm{n+1}} - 2\mathbf{U}_{\mathrm{n}} + \mathbf{U}_{\mathrm{n-1}}}{dt^2} \tag{2}$$

The discrete dynamic equation at n+1-th time step is written as:

$$\mathbf{M}\mathbf{U}_{\mathrm{n+1}} = \mathbf{M}\left(2\mathbf{U}_{\mathrm{n}} - \mathbf{U}_{\mathrm{n-1}}\right) - \mathbf{K}\mathbf{U}_{\mathrm{n}}dt^2 - \mathbf{C}\left(\mathbf{U}_{\mathrm{n}} - \mathbf{U}_{\mathrm{n-1}}\right)dt + \mathbf{F}_{\mathrm{n}}dt^2 \tag{3}$$

If the diagonal lumped mass matrix $\mathbf{M}$ is used, the equation is solved explicitly.

2.2 Viscoelastic Artificial Boundary

In order for a finite mesh to represent the response of an infinite field condition, the artificial reflection of seismic waves from bottom and side boundaries should be minimized. Lysmer et al. (1969) introduced a simple procedure of viscous boundary to accomplish this. For the problem of possibly bigger error and low frequency instability brought by viscous boundary, viscous-elastic artificial boundary is proposed (Liu et al. 1998). The implementation of viscous-elastic artificial boundary involving adding springs and dampers at each of the nodes that make up the bottom and the sides of the finite model, is suggested, as shown in Figure 1 and Figure 2.

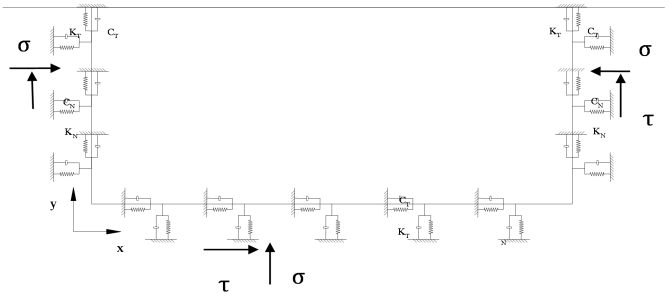

Figure 1. Finite model with viscoelastic artificial boundary

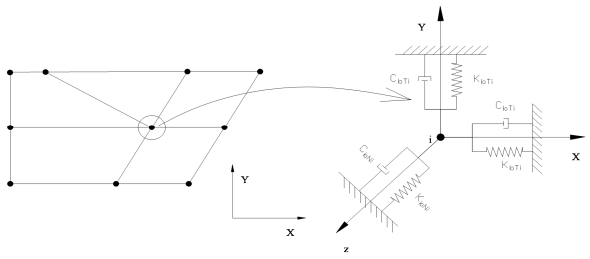

Figure 2. Schematic diagram of 3 dimension viscoelastic artificial boundary

This boundary condition is applied at the far-end boundary of the foundation in three-dimensional space given as:

$$\sigma = K_{\mathrm{n}} u + C_{\mathrm{n}} \dot{u}\,,\ \tau_1 = K_{\mathrm{s}} v + C_{\mathrm{s}} \dot{v}\,, \tau_2 = K_{\mathrm{s}} w + C_{\mathrm{s}} \dot{w} \tag{4}$$

Where σ and τ are the normal and shear tractions; u, v, and w are the displacement of normal and two shear components; $\dot{u}$, $\dot{v}$, and $\dot{w}$ are the velocity of normal and two shear components; K_{n} and K_{s} are the spring coefficient of normal and shear components; C_{n} and C_{s} are the damping coefficient of normal and shear components; K and C are given as:

$$K_{\mathrm{n}} = \frac{E}{2r}\,, K_{\mathrm{s}} = \frac{G}{2r} \tag{5}$$

$$C_{\mathrm{n}} = \rho c_{\mathrm{p}}\,, C_{\mathrm{s}} = \rho c_{\mathrm{s}} \tag{6}$$

Where r is the distance from wave source to boundary; E is modulus of elasticity; G is shear modulus of elasticity; ρ is density ; c_{p} is pressure wave velocity; c_{s} is shear wave velocity; c_{p} and c_{s} are given as:

$$c_{\mathrm{p}} = \sqrt{\frac{(1-\nu)E}{(1+\nu)(1-2\nu)\rho}}\,, c_{\mathrm{s}} = \sqrt{\frac{E}{2(1+\nu)\rho}} \tag{7}$$

Where ν is Poisson's ratio.

2.3 Contact Model Based On Lagrange Multiplier Method

Many models have been used to consider the nonlinear behavior of joints of arch dams (Clough 1980; Niwa et al. 1982; Fenves et al. 1992; Chen 1994; Zhang et al. 1998; Lau et al. 1998; Zhang et al. 2000; Lin et al. 2005; Pan 2015). Most of these models can't strictly meet no penetration condition in

normal direction and stick condition in tangential direction of joints owing to the introduction of penalty function or exponential relationship between force and displacement. Contact model based on Lagrange multiplier can strictly meets the above conditions of joints and simulate the opening, bonding, and sliding of joints.

Let $\mathbf{A}=\mathbf{M}$, $\mathbf{F}=\mathbf{M}\left(2\mathbf{U}_{\mathrm{n}}-\mathbf{U}_{\mathrm{n-1}}\right)-\mathbf{K}\mathbf{U}_{\mathrm{n}}dt^{2}-\mathbf{C}\left(\mathbf{U}_{\mathrm{n}}-\mathbf{U}_{\mathrm{n-1}}\right)dt+\mathbf{F}_{\mathrm{n}}dt^{2}$, $\mathbf{U}=\mathbf{U}_{\mathrm{n+1}}$, and Equation 3 is written as:

$$\mathbf{A}\mathbf{U}=\mathbf{F} \tag{8}$$

The equation including the contact force is written as:

$$\mathbf{A}\mathbf{U}=\mathbf{F}-\mathbf{B}\boldsymbol{\lambda} \tag{9}$$

Where, $\mathbf{B}$ is constraint matrix of contact surface, $\boldsymbol{\lambda}$ is contact force vector.
Displacement constraint equation on contact surface is written as:

$$\mathbf{B}^{\mathrm{T}}\mathbf{U}=\boldsymbol{\gamma} \tag{10}$$

Where, $\boldsymbol{\gamma}$ is displacement constraint vector on contact surface.

The introduction of transformation matrix $\mathbf{T}$ between global coordinate and local coordinate is as follows:

$$\begin{cases}\boldsymbol{\gamma}^{\mathrm{l}}=\mathbf{T}\boldsymbol{\gamma}\\ \boldsymbol{\gamma}=\mathbf{T}^{\mathrm{T}}\boldsymbol{\gamma}^{\mathrm{l}}\\ \boldsymbol{\lambda}^{\mathrm{l}}=\mathbf{T}\boldsymbol{\lambda}\\ \boldsymbol{\lambda}=\mathbf{T}^{\mathrm{T}}\boldsymbol{\lambda}^{\mathrm{l}}\end{cases} \tag{11}$$

The following is derived from Equation 9:

$$\mathbf{U}=\mathbf{A}^{-1}\left(\mathbf{F}-\mathbf{B}\boldsymbol{\lambda}\right) \tag{12}$$

Substitute Equation 9 into Equation 10:

$$\mathbf{B}^{\mathrm{T}}\mathbf{A}^{-1}\left(\mathbf{F}-\mathbf{B}\boldsymbol{\lambda}\right)=\boldsymbol{\gamma} \tag{13}$$

Substitute $\boldsymbol{\lambda}=\mathbf{T}^{\mathrm{T}}\boldsymbol{\lambda}^{\mathrm{l}}$ and $\boldsymbol{\gamma}=\mathbf{T}^{\mathrm{T}}\boldsymbol{\gamma}^{\mathrm{l}}$ into Equation 13：

$$\mathbf{B}^{\mathrm{T}}\mathbf{A}^{-1}\mathbf{B}^{\mathrm{T}}\mathbf{T}^{\mathrm{T}}\boldsymbol{\lambda}^{\mathrm{l}}=\mathbf{B}^{\mathrm{T}}\mathbf{A}^{-1}\mathbf{F}-\mathbf{T}^{\mathrm{T}}\boldsymbol{\gamma}^{\mathrm{l}} \tag{14}$$

$\mathbf{T}$ left-multiplies by both sides of Equation 14:

$$\mathbf{T}\mathbf{B}^{\mathrm{T}}\mathbf{A}^{-1}\mathbf{B}^{\mathrm{T}}\mathbf{T}^{\mathrm{T}}\boldsymbol{\lambda}^{\mathrm{l}}=\mathbf{T}\mathbf{B}^{\mathrm{T}}\mathbf{A}^{-1}\mathbf{F}-\boldsymbol{\gamma}^{\mathrm{l}} \tag{15}$$

Let $\mathbf{C}=\mathbf{T}\mathbf{B}^{\mathrm{T}}\mathbf{A}^{-1}\mathbf{B}^{\mathrm{T}}\mathbf{T}^{\mathrm{T}}$， $\mathbf{D}=\mathbf{T}\mathbf{B}^{\mathrm{T}}\mathbf{A}^{-1}\mathbf{F}-\boldsymbol{\gamma}^{\mathrm{l}}$， the contact force equation can be written as:

$$\mathbf{C}\boldsymbol{\lambda}^{\mathrm{l}}=\mathbf{D} \tag{16}$$

Flexibility matrix $\mathbf{C}$ in contact force equation is full matrix for the upstream face of dam owing to the

different added mass in three directions, where normal force and tangential force are coupled. Based on Mohor-column friction condition and normal contact condition, contact force equation is solved interactively. The contact force in global coordinate system is got by $\boldsymbol{\lambda} = \mathbf{T}^{\mathrm{T}}\boldsymbol{\lambda}^{\mathrm{l}}$ from the contact force in local coordinate system. The global displacement is got by $\mathbf{AU} = \mathbf{F} - \mathbf{B}\boldsymbol{\lambda}$.

2.4 Constitutive Model

The program includes a variety of constitutive models including concrete damage mechanics model, rock damage mechanics model, and plastic mechanics model. The detailed information is omitted in this paper due to page limit.

3. PARALLELIZATION STRATEGY

The parallelization of nonlinear explicit dynamic finite element simulation on distributed memory computers with domain decomposition and explicit message passing is adopted in this paper.

3.1 Domain Decomposition Method(DDM)

The basic idea of DDM is to divide a whole system into several sub-systems (Lv et al. 1997). The solution of original system can be changed into the solution of several sub-systems, and the communication between sub-systems can be achieved by data transferring. DDM is divided into steps as follows:
(1) The whole model is divided into several sub-models;
(2) The solution of each sub-model is done in each partition;
(3) The solution of the whole model is got by combining the results of each sub-model.

By overlapping the district or not, domain decomposition method is divided into overlapping domain decomposition method (ODDM) and non-overlapping domain decomposition method. The basic theory of ODDM is Schwarz alternating method and data exchange between sub-models is done through the overlapping district, as shown in Figure 3.

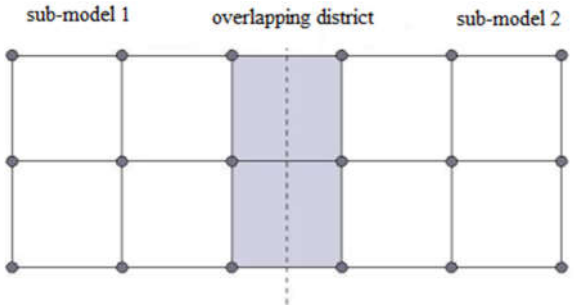

Figure 3. Overlapping district between sub-models (Guo 2014)

3.2 Mesh Partitioning

Generally, two partition concepts for the parallelization of explicit integration scheme include node-cut partitioning and element-cut partitioning (Krysl et al. 2001). In this paper, element–cut partition is adopted for overlapping domain decomposition method. The implementation of mesh partitioning is based on Metis (Karypis 1998). As shown in Figure 4, the nodes of each partition are divided into internal nodes, boundary nodes and external nodes, where solution of internal nodes and boundary nodes is made in each sub-model, and boundary nodes and external nodes are used to exchange information with other sub-models. The boundary nodes of this sub-model are the external nodes of

another one and the external nodes are the boundary of this sub-model. The solution of external nodes is not made in this sub-model.

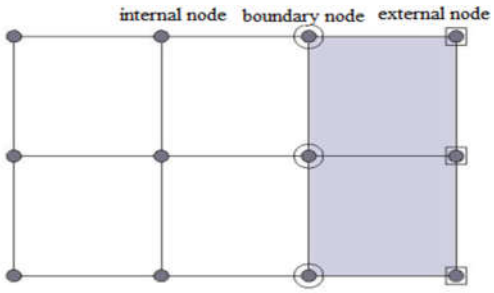

Figure 4. Node distribution diagram in each sub-model (Guo 2014)

3.3 Communication

Currently, the MPI message passing library is used for communication (1995). Parallel architecture uses a master-slave model, consisting of one master processor and several slave processors, as shown in Figure 5. Master processor is a control program that doesn't participate in the computation and is responsible for sending data to slave processors and receiving data from slave processors. All message passing occurs between the master processor and slave processors. There is no message passing between slave processors and slave processors are only responsible for the computation of corresponding sub-model. Message passing is achieved by blocking communication that computation and communication are done sequentially.

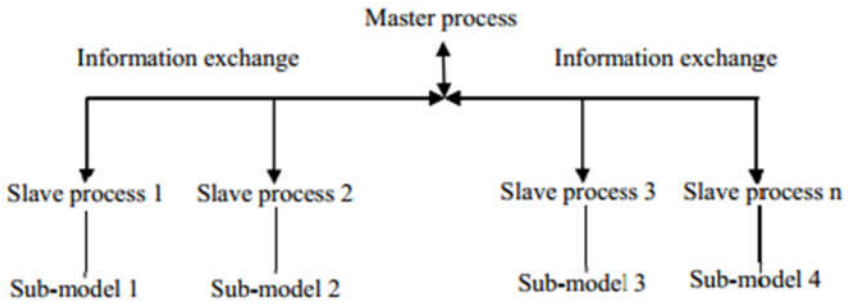

Figure 5. Parallel architecture (Guo 2014)

3.4 Parallel Solution Scheme

Since the mass matrix is diagonal, the wave equation with explicit scheme is decoupled, which has advantage of parallel computation. For the computation of each sub-model, at each time step, the displacement, velocity and acceleration on the boundary of each sub-model are updated by exchanging data of the related overlapping district, and then the displacement, velocity and acceleration of the sub-model are got from the new boundary conditions. Thus, the solution of wave equation with explicit scheme is made without iteration, and the boundary condition is updated by exchanging data at each time step. The parallel computation program is developed based on the combination of Fortran 90 and MPI.

4 PARALLEL PERFORMANCE TEST

The hardware resource of 'TH-1A' is used by internet remote login, and all computation work in this

paper is completed by 'TH-1A' supercomputer which ranked the 2010 world's fastest running speed supercomputer.

Figure 6 shows the finite element model of dam-foundation model for seismic analysis of Shapai high arch dam and domain decomposition into 11 partitions. Considering the damage of the whole dam and the near-field foundation, the maximum finite element grid size of the dam and the near-field foundation is about 2m. The total number of freedom of the finite element system of the whole dam-foundation system is about 1300,000, including the foundation rock region extend to 2 times of the maximum dam height along 3 directions. The time history of input ground motion is 40s that needs a total of 2 million time steps. The performance of parallel computation is tested.

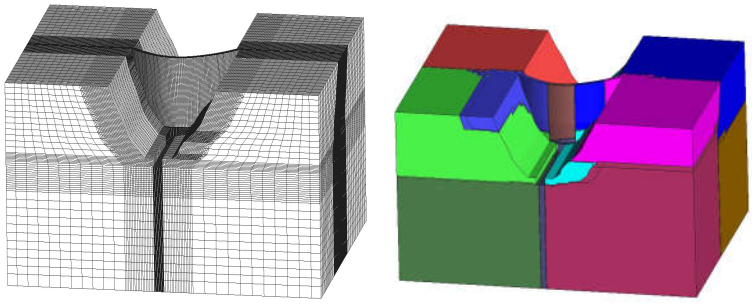

Figure 6. Shapai arch dam-foundation model and domain decomposition into 11 partitions (different color represents different partition)

From Table 1, running time is from 949.4h (39d13.4h) with 1 processor to 18.9h with 192 processors, which shows the parallel computation software has good speedup. With the increase of processors the running time is gradually decreasing and speedup is gradually increasing, which shows the parallel computation program has good scalability.

Table 1. Parallel computation test value

Number of processors	Running time(h)	Speedup
1	949.4(39d13.4h)	1.00
2	499.7	1.90
5	282.8	3.36
11	143.9	6.60
23	73.9	12.85
47	40.6	23.38
95	25.0	38.00
119	22.2	42.77
143	21.1	45.00
191	18.9	50.23

5 SEISMIC STABILITY OF HIGH ARCH DAM-ABUNTMENT ROCK SYSTEM (IWHR 2016; GUO 2016)

The super high arch dam is located in the lower reach of Jinsha River, which is in the transition region

from Tibetan Plateau and Yunnan-Guizhou Plateau to Sichuan Basin, belonging to southwest China with unstable regional geologic structure, complex geological condition and strong tectonic activity. The peak acceleration of the maximum design earthquake (MDE) on the bedrock is 406gal and the peak acceleration of the maximum credible earthquake (MCE) on the bedrock is 481gal

A dam-abutment rock-foundation-reservoir dynamic interaction model is established in this paper. The above contact model is adopted to simulate contraction joints of dam and potential sliding surface of dam abutment. The viscoelastic artificial boundary model is adopted to simulate the effect of seismic wave energy propagation to far field. The nonlinear response of the arch dam during earthquake is explored based on time history analysis. It is notable that the abutment stability of arch dam is vital for arch dam seismic safety, thus the dynamic interaction between the dam and the abutment rock block is considered to evaluate seismic stability of the abutment rock block.

5.1 Model construction

The main parameters of dam are shown as Table 2.

Table 2. Basic parameters of the dam

Dam type	**Concrete hyperbolic arch dam**
Crest elevation	834m
Maximum dam height	289m
Crest centreline chord	709m
Normal water level	825m
Thickness-height ratio	0.218
Chord-height ratio	2.453

As shown in Figure 7 and Figure 8, the total number of nodes, elements, and DOFs are 68637, 60238 and 205911 respectively, including 28 contraction joints and several dam abutment sliding surfaces.

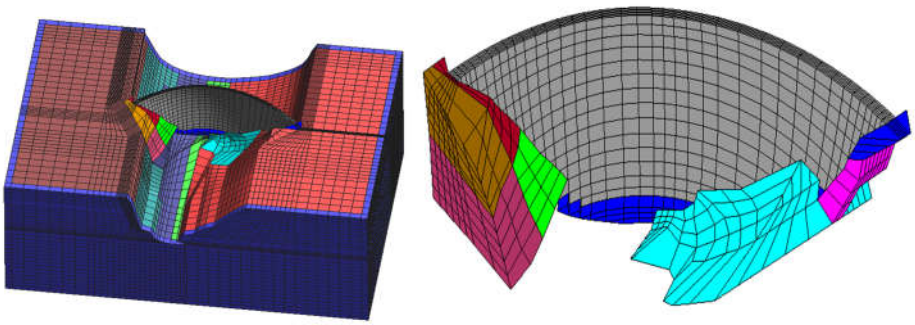

Figure 7. Dam-abutment rock-foundation model and dam-abutment rock model

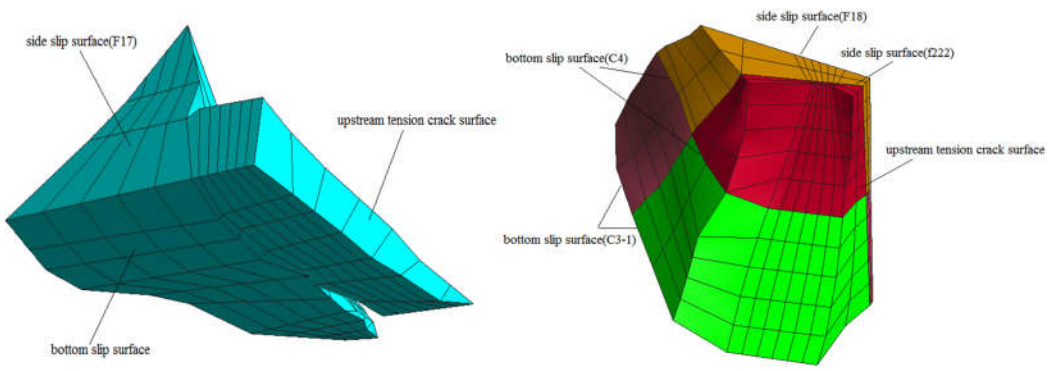

Figure 8. Abutment rock block of left bank and right bank

The main load applied includes up and down water pressure, sediment pressure, weight load, temperature and earthquake load. The elevation of upstream normal water level, downstream normal water level and sediment level is 825m, 604m and 878m respectively. PGA for MDE and MCE is 406gal and 481gal respectively. The normalized artificial waves of input ground motion in three directions are shown as Figure 9. The detailed information including material parameters is omitted in this paper due to page limit.

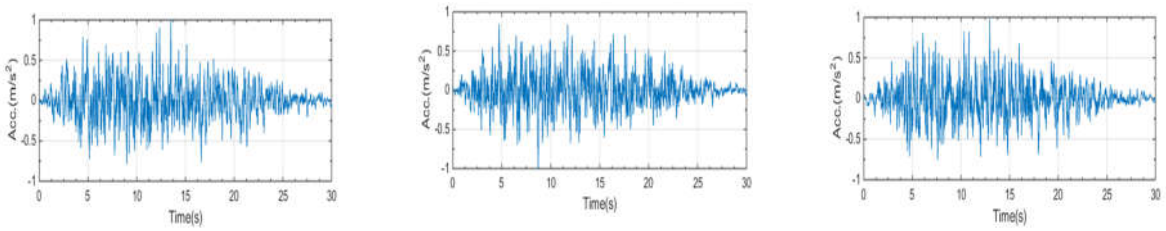

Figure 9 Artificial seismic wave
(from up to down: cross river direction, river along direction, vertical direction)

5.2 Calculation results and analysis

From Figure 10, it can be seen that the slippage of bottom slip surface of left bank and right bank is less than 2.5cm under MCE and it's stable after earthquake, which shows the abutment rock block can resistant thrust force from the dam. From Figure 11, it can be seen that the slippage of bottom slip surface C4 of right bank keeps increasing continuously under overload factor 1.7 of MDE which shows the abutment rock block of right bank is unstable and can't resistant thrust force from the dam, which is unacceptable for high arch dam.

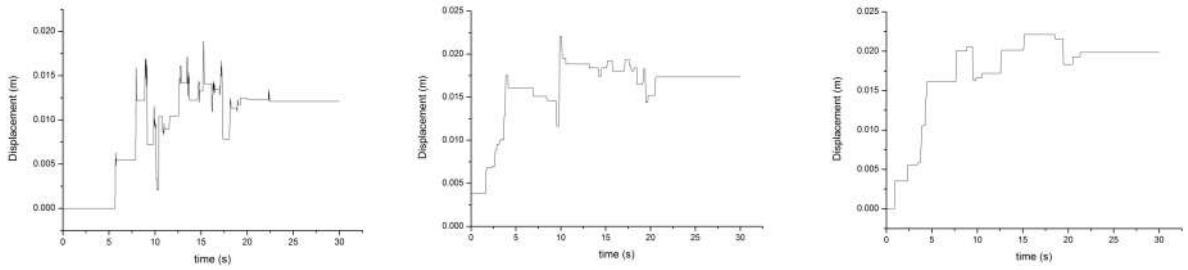

(a) (b) (c)

Figure 10. The time history of slippage of: (a) bottom slip surface of left bank abutment rock block under MCE; (b) bottom slip surface(C4) of right bank abutment rock block under MCE; (c) bottom slip surface(C3-1) of right bank abutment rock block under MCE

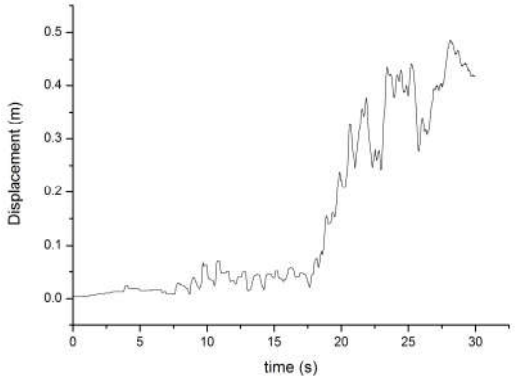

Figure 11. The time history of slippage of bottom slip surface C4 of right bank abutment rock block under overload factor 1.7 of MDE

6 ELABORATE SIMULATION OF SEISMIC DAMAGE OF DAM (IWHR 2017)

Figure 12 shows the finite element model for seismic damage of a high arch dam. Considering the damage of the whole dam, the maximum finite element grid size of the dam is about 2m. The total number of freedom of the finite element system of the whole dam-foundation system is about 3500,000, including the foundation rock region which extends to 2 times of the maximum dam height along 3 directions. Due to page limit, the detailed information of model and load condition is omitted.

Figure 12. Finite element model of a high arch dam for seismic damage analysis

Figure 13 shows the damage state of crown cantilever under earthquakes of different overload factors. It can be seen that the dam body has no damage under design earthquake and has local damage at the upper part of downstream surface in addition to dam heel area and the intersection of dam and pier under MCE. The damage area and damage degree of dam body begin to aggravate when overload factor increases to 1.6~1.8 and the penetrating crack begins to appear through upstream and downstream face. The dam has seriously damaged and is difficult to repair.

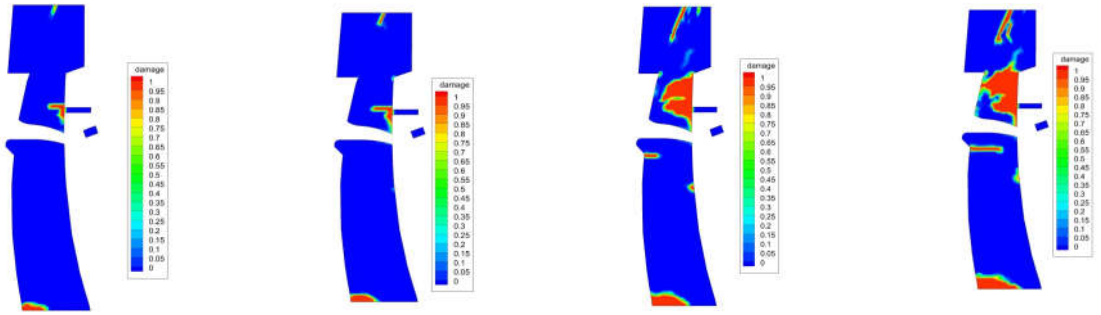

MDE | MCE | Overload factor 1.6 of MDE | Overload factor 1.8 of MDE

Figure 13. Dam damage under earthquakes of different overload factors

7. CONCLUSIONS

(1) The dynamic analysis model including explicit dynamic finite element method, viscoelastic artificial boundary, contact model, and nonlinear constitutive model is formulated. The detailed information of nonlinear constitutive model is omitted due to page limit.

(2) The parallelization of nonlinear explicit dynamic finite element simulation on distributed memory computers with domain decomposition and explicit message passing is formulated. The paralleling strategy including ODDM, mesh partitioning, communication, and parallel solution scheme is formulated subsequently.

(3) The described parallel computation program has been demonstrated to have good speedup and scalability.

(4) In the first application, the attention has been focused on the stability of dam abutment rock block which is vital for seismic safety of high arch dams. In the second application, the attention has been focused on the seismic damage of dam under different level earthquakes which is another seismic failure mode of high arch dam. The two seismic failure modes of high arch dams including dam abutment instability and severe damage of the dam are revealed.

(5) High performance parallel computation is playing more and more important role in the more realistic prediction of seismic response of high arch dams. Due to the limit of pages and time, only part of engineering application achievements by PSDAP is given in this paper. Meanwhile, authors are actively working with experts in high performance computation to further improve the performance of large-scale computation.

8. ACKNOWLEDGMENTS

This paper has obtained the financial support from the national key research and development program (grant number 2017YFC0404903), national natural science foundation (grant number 51709283), and State Key Laboratory of Simulation and Regulation of Water Cycle in River Basin (grant number 2016CG03). The authors are grateful for these supports.

9. REFERENCES

Belytschko T, Plaskacz E J, Chiang H Y (1991). Explicit finite element methods with contact-impact on SIMD computers. *Computing Systems in Engineering*, 2(2):269-276.

China Institute of Water Resources and Hydropower Research, China earthquake Disaster Prevention Center (2016). Seismic safety analysis and evaluation of Baihetan arch dam. (in Chines)

China Institute of Water Resources and Hydropower Research，China earthquake Disaster Prevention Center (2017). Seismic safety analysis and evaluation of Mengdigou arch dam. (in Chines)

Clough R W (1980). Nonlinear mechanisms in the seismic response of arch dams. *International Research Conference on Earthquake Engineering*, Skopje, Yugoslavia.

Chen H (1994). Model test and program verification on dynamic behavior of arch dam with contraction joints. Report No. SVL-94/2 IWHR.

Clinckemaillie J, Elsner B, Lonsdale G, et al (1997). Performance Issues of the Parallel Pam-Crash Code. *International Journal of High Performance Computing Applications*, 11(1):3-11.

Danielson K T, Namburu R R (1998). Nonlinear dynamic finite element analysis on parallel computers using FORTRAN 90 and MPI. *Advances in Engineering Software*, 29(3–6):179-186.

Fenves G L, Mojtahedi S, Reimer R B (1992). Effect of Contraction Joints on Earthquake Response of an Arch Dam. *Journal of Structural Engineering*, 118(4):1039-1055.

Fahmy M W, Namini A H (1994). A survey of parallel nonlinear dynamic analysis methodologies. *Computers & Structures*, 53(4):1033-1043.

Guo S, Li D, Tu J, Chen H (2014). Seismic damage and failure analysis of arch dam with different material models of foundation, *Proceedings of the 2nd European Conference on Earthquake Engineering and Seismology*, 24-29 August, Istanbul, Turkey.

Guo S, Zhai E, Chen H (2016), Seismic vulnerability analysis of a super high arch dam in China, *Proceedings of Hydro 2016*, 10-12 October, Montreux, Switzerland.

Hoover C G, Degroot A J, Maltby J D, and Procassini R J (1995). ParaDyn-DYNA3D for massively parallel computers. Engineering, Research, Development and Technology FY94, Lawrence Livermore National Laboratory, UCRL 53868-94.

Krysl P, Bittnar Z (2001). Parallel explicit finite element solid dynamics with domain decomposition and message passing: dual partitioning scalability. *Computers & Structures*, 79(3):345-360.

Lysmer J, Kuhlemeyer R L (1969). Finite dynamic model for infinite media. *Journal of the Engineering Mechanics Division*, 95: 759 – 877.

Lv T, Shi JM, Lin ZB (1992), Decomposition algorithm, Science press, Beijing, pp 1-10.

Liu JB, Lu YD(1998), A direct method for analysis of dynamic soil-structure interaction. *China Civil Engineering Journal*, 31(3):55-64.

Lau D T, Noruziaan B, Razaqpur A G (1998). Modeling of contraction joint and shear sliding effects on earthquake response of arch dams. *Earthquake Engineering & Structural Dynamics*, 27(10):1013-1029.

Lin G, Hu Z (2005). Earthquake safety assessment of concrete arch and gravity dams. *Earthquake Engineering and Engineering Vibration*, 4(2): 251–64.

Malone J G, Johnson N L (1994). A parallel finite element contact/impact algorithm for nonlinear explicit transient analysis: Part I—The search algorithm and contact mechanics. *International Journal for Numerical Methods in Engineering*, 37(4):559-590.

Malone J G, Johnson N L (1994). A parallel finite element contact/impact algorithm for nonlinear explicit transient analysis: Part II—Parallel Implementation. *International Journal for Numerical Methods in Engineering*, 37(4):591-603.

Message Passing Interface Forum, MPI (1995). A message passing interface standard. University of Tennessee.

Karypis G (1998). Metis home page, www-users.cs.umn.edu./~karypis/metis. .

Niwa A, Clough R W (1982). Non-linear seismic response of arch dams. *Earthquake Engineering & Structural Dynamics*, 10(2):267-281.

Namburu R R, Turner D A, Tamma K K (1995). An effective data parallel self-starting explicit methodology for computational structural dynamics on the connection machine CM-5. *International Journal for Numerical Methods in Engineering*, 38(19):3211-3226.

Pan J, Xu Y, Jin F (2015). Seismic performance assessment of arch dams using incremental nonlinear dynamic analysis. *European Journal of Environmental and Civil Engineering*, 19(3):305-326.

Plimpton S, Attaway S, Hendrickson B, Swegle J, Vaughan C, and Gardner D (1996), Transient dynamics simulation: parallel algorithms for contact detection and smoothed particle hydrodynamics. In *Proceedings of SuperComputing 96*, Pittsburgh, PA, 1996.

Zhang C, Xu Y, Jin F (1998). Effects of soil-structure interaction on nonlinear response of arch dams. *Developments in Geotechnical Engineering*, 83(98):95-114.

Zhang C, Xu Y, Wang G, et al (2000). Non-linear seismic response of arch dams with contraction joint opening and joint reinforcements. *Earthquake Engineering & Structural Dynamics*, 29(10):1547-1566.